Comparison of Different Techniques for Modelling of Flow Field and Homogenization in Stirred Vessels*

M. MOŠTĚK**, A. KUKUKOVÁ, M. JAHODA, and V. MACHOŇ

Department of Chemical Engineering, Faculty of Chemical Engineering, Institute of Chemical Technology, CZ-166 28 Prague
e-mail: michal.mostek@vscht.cz

Received 1 April 2005

Application of different simulation techniques to predict flow field and tracer distribution in a stirred tank was investigated. Impeller motion was explicitly modelled using the Multiple Reference Frames technique (steady-state simulation of the impeller motion) and the Sliding Mesh model (unsteady-state simulation), implemented in the FLUENT code. Simulations were performed for turbulent flow regime using the standard k-ε turbulence model.

Already, using the steady-state simulation approach fairly good prediction of the tracer homogenization in the vessel stirred with the pitched blade turbine was obtained. Simulation results were further improved using the Sliding Mesh model. However, the use of dynamic simulation was about 100 times more time-demanding in contrast to simulation based on the Multiple Reference Frames with the "frozen" flow field.

Mechanically agitated tanks are widely used throughout the process industries for mixing of single or multiphase fluids. Mixing is a fundamental unit operation which has influence on blending, transport, and reaction phenomena and consequently on power consumption and operating efficiency. The efficiency of mixing operations has a big impact on product quality and production costs. One of the most crucial parameters is mixing time, the time to achieve complete homogenization of inserted tracer or time to mix different reactants fed into a tank. Ability of prediction of mixing times for different vessel and impeller configurations is still based mainly on empirical correlations obtained from earlier measurements at some locations in the tank using conductivity probes.

Current CFD methods based on the Reynolds averaged Navier—Stokes approach can provide complete picture of the homogenization process. However, it was shown that the mixing times obtained using this approach do not predict real mixing times with sufficient accuracy. It is therefore essential to compare this approach directly with experimental homogenization data measured in the stirred vessel *via* tracer distribution comparison and not only with computed mixing times.

Early mixing simulations relied on experimentally obtained boundary conditions which were needed to substitute computationally expensive rotation of impellers (*Ranade et al.* [1], *Bakker* and *Fasano* [2]), but this was not fully predictive approach.

Fully predictive simulations of mixing time mainly use either the Sliding Mesh SM (*Murthy et al.* [3]) or the Multiple Reference Frame MRF (*Luo et al.* [4]) approaches. The Sliding Mesh approach is a fully transient approach, where the rotation of the impeller is explicitly taken into account. On the other hand, the Multiple Reference Frames approach predicts steady-flow field for a fixed position of the impeller relative to the baffles. The SM approach is more accurate but it is also much more time-consuming than the MRF approach.

Sliding Mesh simulation of a stirred tank content homogenization was first published by *Jaworski* and *Dudczak* [5]. The authors used the standard k-ε model and the standard wall functions for simulations. Predicted temporal variation of the average tracer concentration at four control volumes was found to vary between the minimum and maximum concentration of the tracer in the tank (experimental data by *Khang* and *Levenspiel* [6]).

Osman and *Varley* [7] studied the mixing time in an unbaffled vessel with a Rushton turbine using the MRF approach. The predicted mixing time was found to be up to two times higher than the experimental one and the authors attributed the discrepancies to the underestimation of the mean velocity compo-

*Presented at the 32nd International Conference of the Slovak Society of Chemical Engineering, Tatranské Matliare, 23—27 May 2005.

**The author to whom the correspondence should be addressed.

nents near the Rushton turbine. *Jaworski et al.* [8] studied homogenization in a baffled vessel stirred by a dual Rushton impeller using the MRF approach. Converged solution of the flow field was then used as an input for the solution of the scalar transport equation using the SM approach in order to simulate the time-dependent mixing process, but not continuing the computation of the flow field. The predicted mixing time was found to be 2—3 times higher than the measured values, in agreement with [7]. The authors of [8] attributed inaccuracies to underprediction of the mass exchange between the recirculation zones generated by the Rushton turbines and wrongly predicted tangential velocity field. The same authors (*Bujalski et al.* [9]) also performed these simulations with denser grid in the regions of high velocity gradients and with more converged solution, while solving the transient scalar transport equation in a stationary reference frame. They obtained improved results but still the mixing time was overpredicted by about two times. In contrast to these papers, *Shekhar* and *Jayanti* [10] successfully simulated flow field and mixing characteristics in an unbaffled vessel stirred by a paddle impeller using low-Reynolds k-ε model for rather low Reynolds numbers.

Objective of the present work is to compare experimental and simulated data based on the velocity field, power and pumping numbers, and concentration curves prediction. The main focus is on comparison of impacts of the previously described approaches on concentration curves and mixing time prediction in a vessel stirred by one 45° pitched 6-bladed impeller (PBT).

THEORETICAL

Three-dimensional simulations were performed using the Computational Fluid Dynamics (CFD) code FLUENT, version 6.2, a finite-volume based fluid dynamics analysis program, which solves nonlinear set of equations formed by discretization of the continuity, the tracer mass balance, and the Reynolds averaged Navier—Stokes conservation equations. Turbulence was modelled using the standard k-ε model in conjunction with logarithmic wall functions.

For the mixing simulations performed, the computational mesh consisted of two parts: inner rotating cylindrical volume enclosing the impeller and part of the shaft, and outer stationary volume filling the rest of the vessel. Origin of the cylindrical coordinate system of this 0.29 m vessel was in the centre of the liquid surface in the vessel. Location of the interface between the two volumes was set in the middle between the impeller tip and the edge of the baffles ($r = 0.0817$ m) in the radial direction and between $z = 0.158$ m and $z = 0.229$ m in the axial direction, which is about one impeller width (0.02 m) above and below the impeller blades. It can be assumed that the flow repeats itself in 180° sectors; therefore the calculation of the flow field can be reduced to just one half of the vessel. However, in order to calculate homogenization of the tracer precisely, simulation of the whole vessel had to be carried out.

Table 1. Details about the Grid Used for Simulation

Grid density in the tank	r	43
	θ	228
	z	99
Grid density on the impeller blade	r	9
	θ	3
	z	6
Number of cells in the rotating section		113484
Number of cells in the stationary section		730080
Total number of cells in the vessel		843564
Average cell volume, V_c/cm^3		0.022

A structured grid composed of hexahedral cells was made in Gambit 2.2 pre-processor. The vessel volume was decomposed to many little volumes to make a grid usable for map meshing. Two symmetry planes were used in the vessel. One was used at the liquid surface to easily simulate the free surface and to avoid the need of two-phase simulation. The second one corresponded to lateral surface of a thin cylinder, which was used from the bottom of the shaft to the tank bottom. With volume decomposition and symmetry planes, structured grid was made. Grid was made similar to MixSim 1.7, another Fluent pre-processor (see *Moštěk et al.* [11]), but denser (MixSim had a limitation of grid size to about 400,000 cells). Details about the grid are summarized in Table 1. The grid density was carefully tested by *Kukuková* [12] and it was assumed that the solution of flow field is grid-independent (solution is not changing with higher number of cells).

First simulation of the flow field was performed using MRF approach. Material properties for water and boundary conditions were set (*e.g.* the rotational speed of impeller, $N = 5\ \mathrm{s}^{-1}$). Converged solution was obtained (all residuals were constant and below 10^{-6}) using the second-order upwind discretization scheme. Then the flow field was "frozen" and unsteady solution of passive scalar equation was solved only, with a time step equal to 0.01 s. The tracer was defined with the same properties as water. It was introduced below the liquid surface opposite to the probe in a region, which corresponded to the experimental point of tracer feeding. Molecular diffusivity coefficient was assumed to be equal to $10^{-9}\ \mathrm{m}^2\ \mathrm{s}^{-1}$; value typical for liquids. Turbulent Schmidt number was kept default, $Sc_t = 0.7$. Mass fraction of the tracer was recorded at a position corresponding to a position of the real probe. At each time step, around 10 iterations were computed to achieve convergence (maximum number of iterations per time step was set to 20 and residual limit was set to 10^{-7}). About 15 s of real time was

simulated, when the mass fraction of the tracer at the specified location no longer varied with the time.

To compare the results obtained using the more computationally demanding Sliding Mesh approach, two simulations with different time steps were performed. In this case, the converged solution of MRF was used as a starting point. The first simulation of SM was performed with a time step equal to 0.001 s (each revolution of the impeller takes 200 time steps). During computations, 10 locations for recording of axial velocity below the impeller were specified, to see the variation of axial velocity in time and to stop the computation when the pseudo-steady-state solution was obtained. The axial velocity profile was also used in post-processing to compare simulated and experimental profile. This solution was obtained after 50 s of real time, *i.e.* after 250 revolutions of the impeller. For each time step, the solution was converged after 15 iterations (residuals were set to 10^{-4}). During the computations of the passive scalar equation, the equations for the computation of the flow field were still turned on (set-up was similar to MRF). This was the most computationally expensive approach.

It is also possible to solve the tracer distribution in the same way as with the "frozen" velocity field (as in the case of MRF simulation). Then, similar simulation strategy on improved flow field could be adopted to see its effect on the simulation solution. Both computational procedures were performed and the results were compared.

To test the effect of time step used during the SM computations, a simulation with time step equal to 0.01 s was performed. The results (pseudo-steady-state solution) were obtained after 120 s of real time (600 revolutions of the impeller). In all cases, the simulations of homogenization procedure were computed for 15 s of the real time.

In order to compare with experimental data, all dimensional data were recomputed to dimensionless concentration curves, according to the relation

$$c^*(t) = \frac{x(t)}{x(t_{\mathrm{end}})} \qquad (1)$$

where $c^*(t)$ is the tracer dimensionless concentration at the time t, $x(t)$ the corresponding mass fraction of the tracer, and $x(t_{\mathrm{end}})$ the mass fraction of the tracer at the end of simulation.

EXPERIMENTAL

Experiments were carried out in a fully baffled cylindrical vessel. The flat-bottomed vessel had a diameter of $T = 0.29$ m. The vessel, equipped with one impeller, was filled with water ($\rho = 1000$ kg m^{-3}, $\mu = 1$ mPa s) to a height H equal to T. The off-bottom clearance of the impeller was one third of the vessel diameter, $C = T/3$. Impeller was attached to a centric shaft, moving in the clockwise direction with a

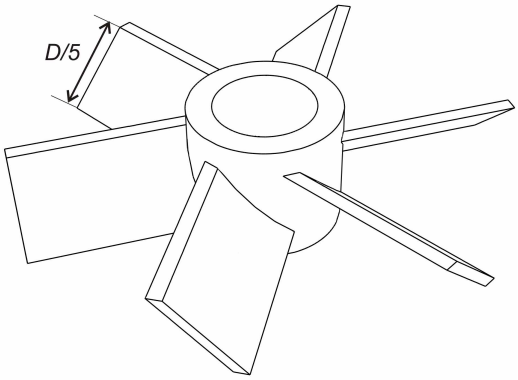

Fig. 1. Scheme of the used impeller.

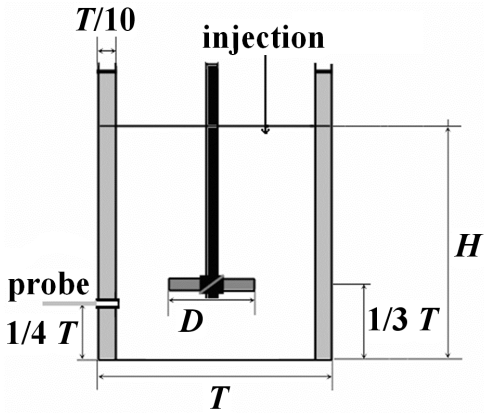

Fig. 2. Experimental set-up.

constant rotational speed (N) of 5 s^{-1}, which corresponds to Reynolds number (Re) of 4×10^4. The shaft ended just below the impeller hub.

For agitation, a 45° pitched 6-bladed turbine (PBT) with a diameter of $D = T/3$ was used. Its blades were 0.0025 m thick and $0.2\,D$ wide. Diameter of the impeller hub was 0.03 m and its height was 0.02 m. The sketch of the impeller used is shown in Fig. 1.

For measurement of concentration curves and times of homogenization (mixing times), one conductivity probe together with a pneumatic injection device was used. Probe consisted of a Perspex tube body with two platinum wires. The probe was placed between the baffles, with off-bottom clearance of $T/4$ and at a distance of $T/20$ from the vessel wall. Approximately 10 cm^3 of the tracer (saturated solution of NaCl) were injected into the bulk. It was injected just below the free surface, at a horizontal distance of $T/4$ from the vessel wall, opposite the probe. The experimental set-up is shown schematically in Fig. 2.

Output signal from the probe was processed by a conductivity meter, digitalized by A/D converter and registered by a computer for further processing. Registered values of voltage from the conductivity meter

were directly proportional to the tracer concentration. For each set-up, 15 measurements were carried out. The measured concentration curve was recomputed to dimensionless concentration curve according to the following equation

$$c^*(t) = \frac{c(t) - c(0)}{c(t_{\mathrm{end}}) - c(0)} \qquad (2)$$

where $c^*(t)$ is the dimensionless concentration at a given time, $c(t)$ concentration in the vessel at the same time, $c(0)$ concentration in the vessel at the beginning of the experiment, and $c(t_{\mathrm{end}})$ the concentration in the vessel at the end of experiment, when the concentration was not changing with time anymore.

From all measurements, an average curve was computed and for the comparison of simulations with experiments, experimental range was made. The range was created as the average value plus or minus the standard deviation.

The time of homogenization (mixing time), t_{95}, was determined from the averaged concentration curve. It is defined as the time from the introduction of the tracer to the time, when the tracer concentration at the probe position has reached and remains within a certain range of the final value. The range was set to ± 5 % (t_{95}).

RESULTS AND DISCUSSION

Assessment of the effect of solution strategy on predicted values of the mean velocity was accomplished first. Plots of radial profiles of mean axial velocity were created in order to graphically compare the predicted (CFD) and experimental (LDV) data.

When using the MRF approach, all radial profiles of the mean axial velocity were tangentially averaged (except the velocities near the vessel wall) in order to prevent incorrect comparison of the profiles caused by steady solution of the impeller motion, because local velocity value depends on the position of the impeller blade. During the simulation with SM approach, mean axial velocities were recorded with the aim to establish the time when the solution "pseudo" steady state is reached, but also for post-processing.

Axial velocity profiles were measured by *Ranade* and *Joshi* [13] in a distance of 0.01 m below the lowest edge of the impeller blade, from the shaft axis to the vessel wall. Thirteen locations were chosen within the experimental range, in radial direction from $r = 0.02$ m to $r = 0.14$ m.

Comparison of the simulated and experimental data is depicted in Fig. 3. Simulated dimensionless mean axial velocity profiles are similar to the experimental profile (squares). Best agreement can be found using the Sliding Mesh approach with time step equal to 0.001 s (dashed line with triangles). Simulation using SM with the time step of 0.01 s was found to be

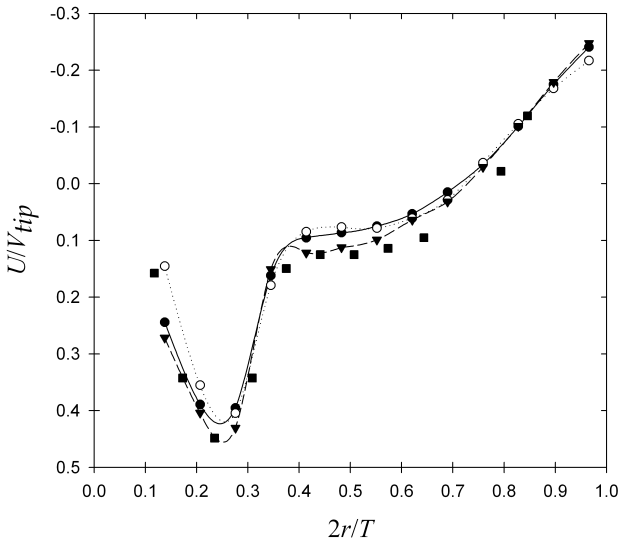

Fig. 3. Comparison of the measured and computed dimensionless mean axial velocity (U/V_{tip}) *vs.* dimensionless radial coordinate ($2r/T$): experiment – squares; MRF – filled circles; SM with $ts = 0.01$ s – open circles; SM with $ts = 0.001$ s – triangles.

insufficient (dotted line with filled circles) and the solution obtained with MRF is better (solid line with open circles), but differences can be found below the impeller ($0 < 2r/T < 0.33$). Consequently, the more computationally demanding Sliding Mesh approach can cause a little improvement, when the time step is set to 0.001 s.

Further, from the momentum (torque) defined by

$$P = 2\pi NM \qquad (3)$$

the power numbers on the tank walls and baffles, $Np_{\mathrm{baff+walls}}$, on the shaft and impellers, $Np_{\mathrm{imp+shaft}}$, as well as the power number from the integral of the turbulence energy dissipation rate, Np_ε, were calculated as follows

$$Np_{\mathrm{baff+walls}} = P/(\rho N^3 D^5) \qquad (4)$$

$$Np_{\mathrm{imp+shaft}} = P/(\rho N^3 D^5) \qquad (5)$$

$$Np_\varepsilon = \int \varepsilon/(ND^3) \qquad (6)$$

where P represents the momentum, ρ is the fluid density, N the impeller rotational speed, D the diameter of the impeller, and ε the dissipation rate of turbulence kinetic energy.

Calculated power numbers were compared to the experimental values, which were ranging between 1.47 and 1.73 (see *Kukuková et al.* [14]). Pumping number, *Nq*, was calculated by integrating the mean axial velocity on the plane under the PBT. These data were compared with the experimental ones, which fall into the range of 0.71—0.97.

Table 2. Overview of Computed Power, Np, and Pumping Numbers Nq

Simulation strategy	$Np_{\mathrm{baff+walls}}$	$Np_{\mathrm{imp+shaft}}$	Np_{ε}	Nq
MRF	1.58	1.60	1.19	0.82
SM, $ts = 0.01$ s	1.61	1.44	1.14	0.81
SM, $ts = 0.001$ s	1.61	1.62	1.23	0.83
Experiments		1.47—1.73		0.71—0.97

Power and pumping numbers calculated for both MRF and SM approaches are summarized in Table 2. Power numbers computed from the momentum on the baffles and walls, $Np_{\mathrm{baff+walls}}$, and from the momentum on the impeller and shaft, $Np_{\mathrm{imp+shaft}}$, fall into the range of experimental values except of the data calculated for SM approach with a larger time step $ts = 0.01$ s. In this case, the momentum on impeller was underpredicted and differed from the remaining results. It was found that the SM approach with $ts = 0.01$ s yielded the lowest values of all computed numbers. Slightly higher values were obtained with the MRF approach and the highest values were obtained using the SM approach with a smaller time step of 0.001 s.

Power numbers computed from the integral of the turbulence energy dissipation rate, Np_{ε}, were in all cases underpredicted with the value of about 75 % of the previous power numbers. This fact should be attributed to the character of the used turbulence model. The power numbers characterize the turbulence field prediction in the systems. It is well known that the RANS approach can predict the mean flow reasonably well but invariably underpredicts the turbulent kinetic energy by as much as 50 % [15]. It is expected that this behaviour will certainly affect the predictions of mixing patterns and time.

All computed values of pumping numbers are similar and do not exceed the range of experimental values (0.71—0.97). The results have similar trend to the power numbers.

Fig. 4 represents the comparison of dimensionless concentration curves for all simulation cases with the experimental one. Moreover, the thin dashed lines show the experimental range computed from 15 experiments. The minimum was computed as an average of the dimensionless concentration curves from all experiments minus standard deviation. The maximum is the average plus the standard deviation. The averaged experimental dimensionless concentration curve is represented by the dotted-dashed line.

From Fig. 4 it is evident that the curves simulated with SM approaches with continuing the computation of the flow field together with the equation of passive scalar transport gave different results from those

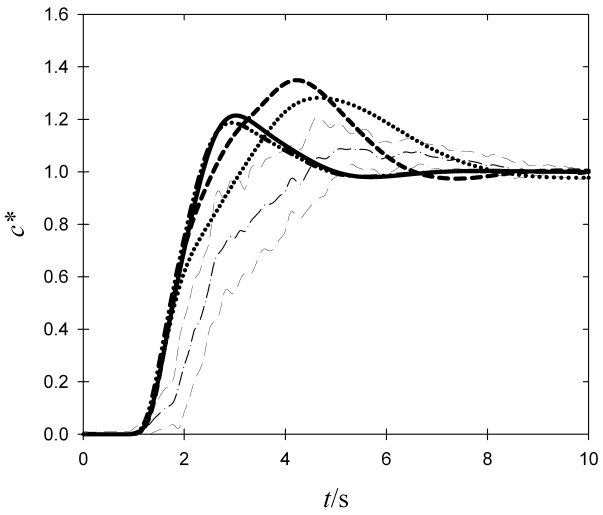

Fig. 4. Comparison of the experimental and computed homogenization curves with different computational strategies: experimental range – thin dotted-dashed line; experimental average – medium dotted-dashed line; MRF – solid line; SM with $ts = 0.001$ s – dotted line; SM with $ts = 0.01$ s – dashed line; SM with $ts = 0.001$ s, frozen – dotted-dotted-dashed line.

calculated for the MRF approach and for the SM approach with "frozen" flow field, the last two being almost identical. Best agreement with the experimental data was observed when the simulation with SM approach and time step 0.001 s was performed, *i.e.* when the flow field equations were solved together with the species transport equation. Similarly to the average experimental curve, the turn at $c^* = 0.7$ was observed in both cases using the SM approach. Homogenization of the vessel content was slightly faster when choosing a bigger time step.

As the results obtained for the two simulations using a "frozen" flow field were similar, the improvement caused by the use of the SM approach did not have a great influence on the tracer distribution in the vessel. Therefore, only the model of impeller rotation solved together with the passive scalar equation improved significantly the computed dimensionless homogenization curves.

Detail of the homogenization curves near the mixing time, t_{95}, is shown in Fig. 5. Prediction of the concentration curve near this point was again more accurate using the SM approaches. Precise simulation of the concentration curve is the most critical for the prediction of mixing times, t_{95}, *i.e.* the time, from which the tracer concentration remains within the range of the final dimensionless concentration ± 5 %. Table 3 presents the comparison of experimental and simulated mixing times.

Again, the best agreement between experimental and simulated data was achieved using SM approach and the smaller time step, when the simulated mixing time was almost identical to the averaged experimen-

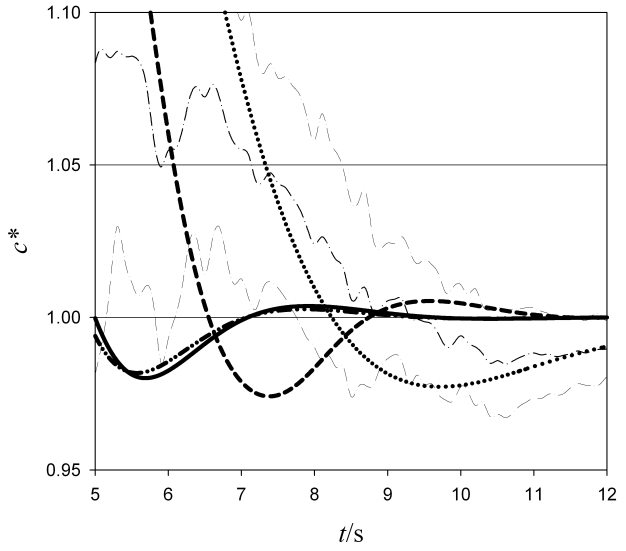

Fig. 5. Detail of comparison of the experimental and simulated concentration curves near the point of mixing time: experimental range – thin dotted-dashed line; experimental average – medium dotted-dashed line; MRF – solid line; SM with $ts = 0.001$ s – dotted line; SM with $ts = 0.01$ s – dashed line; SM with $ts = 0.001$ s, frozen – dotted-dotted-dashed line.

Table 3. Comparison of Experimental and Simulated Mixing Times

	Mixing time, t_{95}/s
Experimental average	7.2
Experimental range	4.9—8.4
MRF	4.43
SM, $ts = 0.001$ s	7.33
SM, $ts = 0.01$ s	6.08
SM, $ts = 0.001$ s, frozen	4.30

tal mixing time. Also the computed mixing time for the SM approach with ten times larger time step fits the experimental one fairly well. On the other hand, the mixing times obtained by the MRF approach, or SM approach with the "frozen" flow field, were not accurate enough, *i.e.* about 40 % underpredicted.

Acknowledgements. This research was supported by the Ministry of Education of the Czech Republic (Grant Research Project MSM6046137306) and the Grant Agency of the Czech Republic (104/03/H141).

SYMBOLS

C	impeller off-bottom clearance	m
c	concentration	mol dm^{-3}
c^*	dimensionless concentration	
D	impeller diameter	m
H	liquid height	m
k	turbulent kinetic energy	m^2 s^{-2}
M	momentum	N m
N	rotational speed	s^{-1}
Np	power number	
Nq	pumping number	
P	power	W
r	radial coordinate	m
Sc_t	turbulent Schmidt number	
T	tank diameter	m
ts	time step	s
t_{95}	mixing time	s
U	mean axial velocity	m s^{-1}
V_c	average cell volume	cm^3
V_{tip}	impeller tip speed	m s^{-1}
x	mass fraction	
z	axial coordinate	m
ε	dissipation rate of turbulent kinetic energy	m^2 s^{-3}
μ	viscosity	Pa s
θ	tangential coordinate	°
ρ	density	kg m^{-3}

REFERENCES

1. Ranade, V. V., Bourne, J. R., and Joshi, J. B., *Chem. Eng. Sci. 46*, 1883 (1991).
2. Bakker, A. and Fasano, J. B., *AIChE Symp. Series 299*, 71 (1994).
3. Murthy, J. Y., Mathur, S. R., and Choudhury, D., *IChemE Symp. Series 136*, 341 (1994).
4. Luo, J. Y., Issa, R. I., and Gosman, A. D., *IChemE Symp. Series 136*, 549 (1994).
5. Jaworski, Z. and Dudczak, J., *Comput. Chem. Eng. 22*, 293 (1998).
6. Khang, S. J. and Levenspiel, O., *Chem. Eng. Sci. 31*, 569 (1976).
7. Osman, J. J. and Varley, J., *IChemE Symp. Series 146*, 15 (1999).
8. Jaworski, Z., Bujalski, W., Otomo, N., and Nienow, A. W., *Chem. Eng. Res. Des. 78*, 327 (2000).
9. Bujalski, W., Jaworski, Z., and Nienow, A. W., *Chem. Eng. Res. Des. 80*, 97 (2002).
10. Shekhar, A. M. and Jayanti, S., *Chem. Eng. Res. Des. 80*, 482 (2002).
11. Moštěk, M., Kukuková, A., Jahoda, M., and Machoň, V., in *Proceedings of the 31st International Conference of the Slovak Society of Chemical Engineering,* Tatranské Matliare, Slovak Republic, 2004.
12. Kukuková, A., *MSc. Thesis.* Institute of Chemical Technology, Prague, 2004.
13. Ranade, V. V. and Joshi, J. B., *Chem. Eng. Res. Des. 68*, 19 (1990).
14. Kukuková, A., Moštěk, M., Jahoda, M., and Machoň, V., *Chem. Eng. Technol.*, in press (2005).
15. Ng, K., Fentiman, N. J., Lee, K. C., and Yianneskis, M., *Chem. Eng. Res. Des. 76*, 737 (1998).